Giant fluidic impedance of nanometer-sized water bridges: Shear capillary force at the nanoscale

Manhee Lee,[1,*] Hyouju Choi,[1] Bongsu Kim,[2,†] and Jongwoo Kim[3]

[1]*Department of Physics, Research Institute for Nanoscale Science and Technology, Chungbuk National University, Cheongju, Chungbuk 28644, Republic of Korea*

[2]*Department of Chemistry, University of California, Irvine, California 92697, USA*

[3]*Korea Research Institute of Chemical Technology, Daejeon 34114, Republic of Korea*

(Received 5 September 2021; accepted 9 May 2022; published 17 June 2022)

We analytically show that the interfacial fluid's molecular dynamics of capillary bridges induces both elastic and dissipative forces to the shearing plane. Surprisingly, the nanometer-sized, liquid-solid contact line of the bridges exerts a giant "shear" force on the solid surface, which is 10^5 higher than the usual viscous interaction and comparable to that of solid-solid direct-contact friction. These results are consistent with previously reported experimental data and may provide clues to longstanding questions on the apparent viscosity of the nanoconfined fluids.

DOI: 10.1103/PhysRevE.105.065108

Nanobridges of water are ubiquitous in nature. Such liquid bridges can form by capillary condensation in nanometric gaps exposed to air [1–3]. The nanometric water bridges induce a capillary force, usually much stronger than other surface interactions such as van der Waals and electrostatic forces [4,5], that may dominate the contact mechanics of solid objects in air [6,7]. This capillary interaction has been extensively investigated for fundamental understanding of liquid-solid interaction [8] and for practical applications such as friction control [9], optical switching [10,11], manipulation of nano-objects [12,13], and self-assembly of colloidal particles [14,15].

In essence, the capillary force originates from the deep negative pressure and the boundary-surface energy of the liquid bridge; the negative pressure produces a normal attractive force on the liquid-solid contact area [blue arrow in Fig. 1(a)] and the surface energy induces a tangential force on the contact line at liquid-solid interfaces [thin red arrows in Fig. 1(a)]. By summing the tangential force around the contact line, we obtain a net attractive force in the normal direction for a symmetrically shaped bridge. The sum of contact-area and contact-line forces is the "normal" capillary force [16]. When the upper surface moves in the lateral direction, the bridge is sheared and distorted; the resulting capillary force can have a nonvanishing horizontal component [Fig. 1(b)]. This "shear" capillary force can directly induce friction between two sliding surfaces that may or may not be in contact [17]. This has direct implications for many natural systems [18], as well as for engineering and industrial processes [19].

While elaborate models of capillary forces have been developed to describe capillary phenomena, nearly all of them describe normal capillary force, i.e., the vertical component of the capillary interaction. Thus, most studies have been limited to examining the normal capillary interactions, though the systems involve shear capillarity. Moreover, the capillary bridges are known to mediate the tip-sample interaction in shear-mode atomic force microscopy (AFM) [20–24], but the physical mechanism of the shear interaction is still elusive. Despite more than one hundred years of research on capillary force [25], the physical origin and analytical formulation of "shear" capillary force is absent.

In this paper, we theoretically investigate the capillary shear interaction with a nanosized liquid bridge, taking into account the fluid's molecular dynamics on the contact line at liquid-solid interfaces. In our theory, we assume that the viscosity of the nanobridges does not change significantly from that of the bulk phase. Instead, we consider the pinning-depinning mechanics of the liquid molecules on the contact line to derive the shear interaction. We analytically present the "apparent" elastic and damping coefficients of the shear capillary force, which are the experimental observables in oscillatory probing techniques such as AFM. As we shall show, the nanometer-sized water bridge yields a giant fluidic impedance given as the sum of the elastic and the dissipative coefficients, which is consistent with previously reported experimental results [20–24]. Furthermore, our model captures three essential characteristics of the shear capillary interaction [17]: (i) finite values of elastic and damping coefficients in the limit of zero modulation amplitude, (ii) the elasticity decaying faster than the damping coefficient with increasing the modulation amplitude, and finally (iii) the logarithmic increment of damping force and the converging elastic force with the amplitude.

In humid air, the nanosized bridges of water can be formed in the nanometric gap between two surfaces by capillary condensation [1–3]. The condensed water induces capillary forces at both the liquid-solid contact area and the liquid-solid contact line (Fig. 1). On the one hand, the pressure inside the nanometric bridge is much smaller than that of the atmosphere; this negative pressure in the bridge generates an

*Corresponding author: mlee@cbnu.ac.kr

†Present address: Samsung Advanced Institute of Technology, 130 Samsung-ro, Yeongtong-gu, Suwon, Gyeonggi 16678, Republic of Korea.

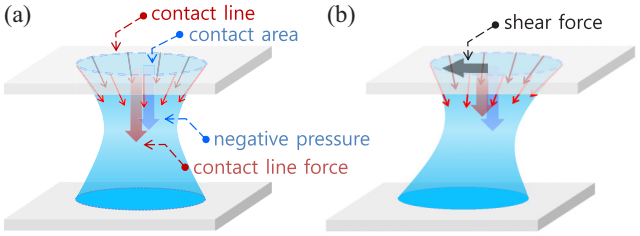

FIG. 1. Normal and shear capillary forces. (a) In humid air, a nanometric water bridge forms in the gap between two surfaces by capillary condensation. The symmetrical capillary bridge exerts a "normal" capillary force (red and blue arrows), which is the sum of the force due to the negative pressure in the bridge (blue arrow) and the force at the liquid-solid contact line (red arrow). (b) If the upper surface moves laterally, the bridge is sheared and the surface experiences a laterally directed "shear" capillary force (grey arrow) as well.

attractive force normal to the contact surface [blue arrow in Fig. 1(a)], with magnitude equal to the pressure times the liquid-solid contact area. On the other, the sum of the tangential forces [thin red arrows in Fig. 1(a)] around the liquid-solid contact line results in a net attractive force normal to the liquid-solid contact interface for an axially symmetric liquid bridge [red arrow in Fig. 1(a)]. However, the situation is more complex when the upper surface moves in a lateral direction [Fig. 1(b)]: the contact angles change, and so do the directions and magnitudes of the tangential forces. Thus, the sum of tangential forces now includes a nonvanishing component in the lateral direction [grey arrow in Fig. 1(b)], which is the shear capillary force.

Let us first suppose that the upper surface moves slowly ($v \approx 0$) in the lateral direction while the liquid-solid contact line remains pinned to the upper surface [Fig. 1(b)]. The liquid-vapor interfacial surface is gradually distorted and the overall interfacial surface energy U_s increases. This leads to a restoring force $F_\mathrm{k} = -dU_s/dx$, where x is the lateral displacement. For simplicity, let us consider a cylindrical column of water with radius R_ψ [Fig. 2(a)]. Under a shear displacement of x, the interfacial energy is given by $4\gamma R_\psi h_\psi E[-(x/h_\psi)^2]$, where γ is the surface tension, E is the complete elliptic integral of the second kind, and h_ψ is the height of the water column. Thus, the restoring elastic force F_k is given by the gradient of the interfacial energy:

$$F_\mathrm{k}(x, v=0) = -4\gamma R_\psi \frac{E[-(x/h_\psi)^2] - K[-(x/h_\psi)^2]}{x/h_\psi}, \quad (1)$$

where K is the complete elliptic integral of the first kind (see Supplemental Material [26] for the detailed derivation).

Next, we consider the shear force at the position of tip plate, $x = 0$, while the tip moves at a velocity v in the lateral direction. If the tip surface is undergoing harmonic oscillation in the x direction, the maximum speed of the tip is $v = wA$ at $x = 0$, where w is the angular frequency of the tip oscillation and A is the oscillation amplitude. Due to the dynamic motion of the plate, the contact line can move along the moving surface, changing the contact angle [27]. This can result in a nonvanishing lateral component of the tangential force even at $x = 0$, depending on the upper plate speed $v = wA$. We can

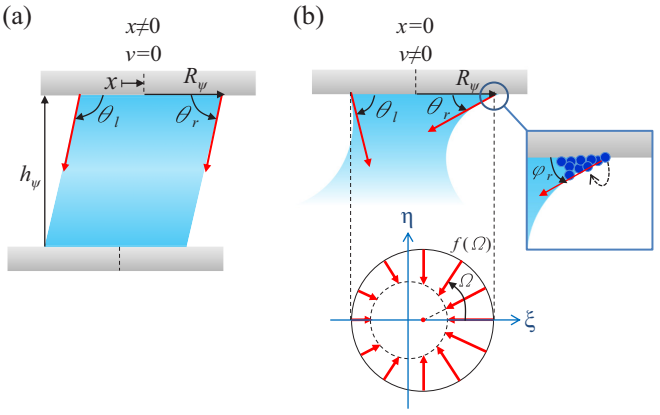

FIG. 2. Shear capillary forces at two states of the tip: (a) the tip (upper surface) velocity $v = 0$ and (b) the tip position $x = 0$. (a) When the tip's position is slowly displaced ($v \approx 0$), the interfacial surface energy U_s dominates the overall shear interaction. The increased surface energy induces a restoring force $F_\mathrm{k} = -dU_s/dx$. A cylindrical column can be used to calculate the surface area and the associated elastic restoring force analytically. (b) When the tip moves with a finite velocity v at position $x = 0$ in the x direction, the liquid-solid contact angles change due to the pinning-depinning dynamics of the contact line (inset). The changing contact angle around the contact line results in unbalanced tangential forces, the lateral components of which add up to a velocity-dependent damping force.

analytically calculate the tip's velocity-dependent damping force F_b by assuming a circular distribution of the horizontal components of the tangential force [Fig. 2(b)]. By horizontal component $f(\Omega)$ at the polar angle Ω in ξ-η coordinate [the blue-colored coordinate frame in Fig. 2(b)] we mean the projection of the tangential force onto the plane of the liquid-solid interface [thin red arrows in Fig. 2(b)]; this clearly varies in magnitude around the circumference of the contact circle in the ξ-η plane. The magnitude and the direction of $f(\Omega)$ are then determined in a way that the force is proportional to the geometrical length l of the red arrow in the ξ-η plane, i.e., $f(\Omega) = \tau l(\Omega)$, where τ is a constant to be determined. As indicated in Fig. 2(b), the outer circle, on which the $f(\Omega)$ acts, has a radius of R_ψ, and the radius of the inner circle is unknown. The two unknowns (the constant τ and the radius of the inner circle) are uniquely determined by the two relations $f(0) = \gamma \cos\theta_r$ and $f(\pi) = \gamma \cos\theta_l$, where θ_r is the dynamic contact angle at $\Omega = 0$, and θ_l at $\Omega = \pi$ [Fig. 2(b)]. By integrating $f(\Omega)$ over $0 \leqslant \Omega < 2\pi$, we formally obtain a force F_b in terms of θ_r and θ_l:

$$F_\mathrm{b} = -\frac{\pi R_\psi}{2}\gamma(\cos\theta_r - \cos\theta_l). \quad (2)$$

If θ_r and θ_l are known, the tip's velocity-dependent damping force F_b at $x = 0$ can be determined.

We can determine θ_r and θ_l by using molecular kinetic theory [28], which relates the dynamic contact angle θ to the relative velocity V of the contact line with respect to the contact surface:

$$V = 2V_0 e^{-U/k_BT} \sinh\left(\frac{\lambda^2\gamma(\cos\theta_\mathrm{eq} - \cos\theta)}{2k_BT}\right), \quad (3)$$

with $V_0 \equiv \lambda k_B T/h$. Here λ is the length of activated jump of fluid's molecules, and U the activation energy of the jump, k_B the Boltzmann constant, T the absolute temperature, h the Planck constant, and $\theta_{\rm eq}$ the equilibrium contact angle. Thus, the dynamics of the contact line is governed by the out-of-balance surface tension force $\gamma(\cos\theta_{\rm eq} - \cos\theta)$ and two parameters, the hopping length λ and the activation energy U.

Since a higher tip velocity could induce larger contact line motion, we assume that the relative velocity V is approximately the same as the tip velocity $v = wA$, i.e., $V = v = wA$ at $x = 0$. Rewriting Eq. (2) as $F_{\rm b} = -(\pi R_\psi/2)\{\gamma(\cos\theta_{\rm eq} - \cos\theta_l) - \gamma(\cos\theta_{\rm eq} - \cos\theta_r)\}$ and using Eq. (3), we obtain the damping force $F_{\rm b}$ as a function of tip velocity v:

$$F_{\rm b}(x=0,v) = -\pi R_\psi \frac{2k_BT}{\lambda^2}\sinh^{-1}\left(\frac{v}{2V_0 e^{-U/k_BT}}\right). \quad (4)$$

We construct the shear capillary force $F_{\rm s}$ at an arbitrary position and velocity of the tip as the superposition of the elastic force, Eq. (1), and the damping force, Eq. (4):

$$F_{\rm s}(x,v) \equiv F_{\rm k}(x,0) + F_{\rm b}(0,v). \quad (5)$$

This assumption implies that the pinning of the contact line changes the liquid-air interfacial energy under shear, which generates the elastic force $F_{\rm k}$ dominating the overall interaction at $x = A$ (or $v = 0$). Further, the pinning-depinning of the contact line induces the dominating dissipative damping force $F_{\rm b}$ at $x = 0$ (or $v = wA$). Therefore, Eq. (5) is an approximation obtained by smoothly interpolating between two force values at $x = 0$ and $x = A$, which is based on the decoupling of position and velocity variables at $x = 0$ and $x = A$.

The expression of shear force, Eq. (5), yields the force coefficients that are expected in the limit of small oscillation. Under small oscillation, materials are expected to exhibit linear response such that force coefficients are "force divided by displacement." Indeed, Eq. (5) results in the elastic coefficient $k_{\rm int} \approx F_s(x=A,v=0)/A = F_{\rm k}(x=A)/A$ and the damping coefficient $b_{\rm int}w \approx F_s(x=0,v=wA)/A = F_{\rm b}(x=0)/A$. In addition, as we shall show in Figs. 3(b) and 4(a), the exact calculation gives very consistent results with experiments [17]: the elastic coefficient $k_{\rm int}$ decays faster than the damping coefficient $b_{\rm int}w$ with increasing the modulation amplitude, and the damping force $b_{\rm int}wA$ logarithmically increases and the elastic force $k_{\rm int}A$ converges to a value with the increment of amplitude A.

Experimentally, the shear capillary interaction can be investigated with probe-based oscillatory techniques, such as AFM [20,29] or use of a surface force apparatus [30,31]. In such measurements, the shear interaction is extracted from dynamic responses of the tip, such as the oscillation amplitude change and the phase shift [32]. With this dynamical information, we finally obtain the apparent elastic and damping coefficients $k_{\rm s}$ and $b_{\rm s}w$ (see Supplemental Material [26]),

$$\frac{k_{\rm s}}{k_0} = \frac{8}{\pi^2\overline{A}^2}\left(\frac{\pi^2}{2}\,{}_3F_2\left[-\frac{1}{2},\frac{1}{2},\frac{1}{2};1,1;-\overline{A}^2\right] - 2\left\{K\left[\frac{1}{2}\left(1-\sqrt{1+\overline{A}^2}\right)\right]\right\}^2\right) \quad (6)$$

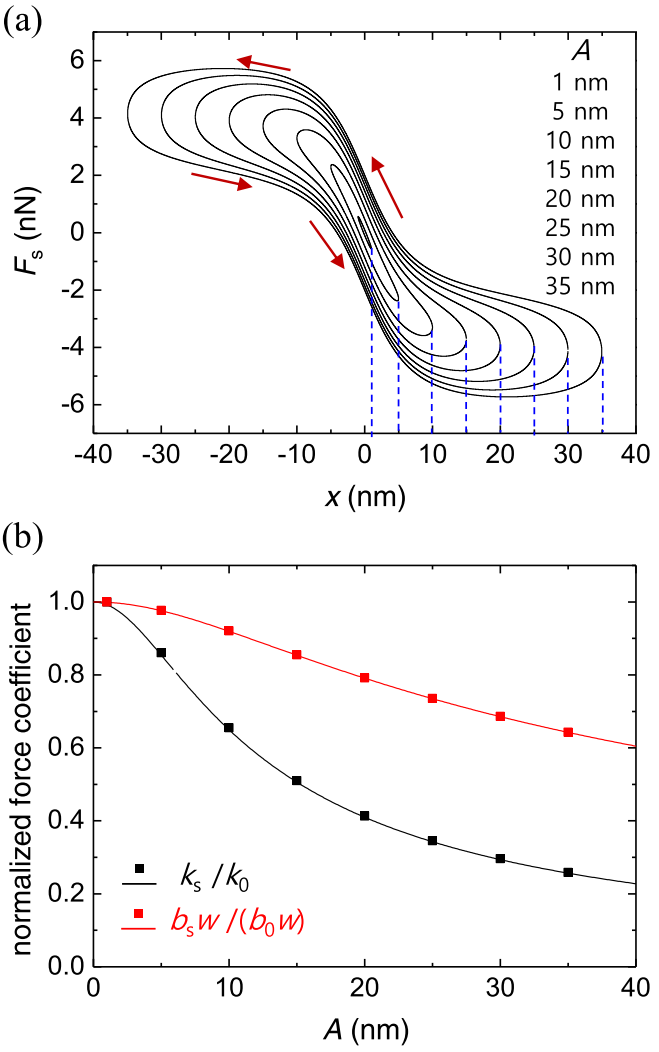

FIG. 3. Shear capillary force F_s and the associated elastic and damping coefficients $k_{\rm s}$ and $b_{\rm s}w$. (a) Shear capillary forces [Eq. (5)] are plotted as a function of the tip position x at different oscillation amplitudes $A = 1, 5, 10, 15, 20, 25, 30, 35$ nm. (b) The black solid curve corresponds to apparent elasticity $k_{\rm s}$ [Eq. (6)] and the red curve to apparent damping coefficient $b_{\rm s}w$ [Eq. (8)]. The black and red colored dots are the results of numerically integrating the force curves shown in (a) (Supplemental Material [26]). We have used typical parameters of capillary-condensed water bridges [17]: $R_\psi = 15$ nm, $h_\psi = 6$ nm, $\lambda = 0.6$ nm, $U = 15k_BT$, and $w/2\pi = 32\,768$ Hz.

$$\text{with } k_0 = \frac{\pi R_\psi}{h_\psi}\gamma, \quad (7)$$

$$\frac{b_{\rm s}w}{b_0 w} = \frac{4}{\pi}\frac{\sqrt{1+a^2}}{a^2}\left\{K\left[\frac{a^2}{1+a^2}\right] - E\left[\frac{a^2}{1+a^2}\right]\right\} \quad (8)$$

$$\text{with } b_0 w = \frac{\pi w R_\psi h}{\lambda^3 e^{-U/k_BT}}, \quad (9)$$

where $\overline{A} = A/h_\psi$, $a = Aw/(2V_0e^{-U/k_BT})$, and ${}_3F_2$ is the generalized hypergeometric function.

As the tip oscillates laterally, the shear force F_s [Eq. (5)] exhibits hysteresis [red arrows in Fig. 3(a)], because the damping-force direction changes sign depending on the

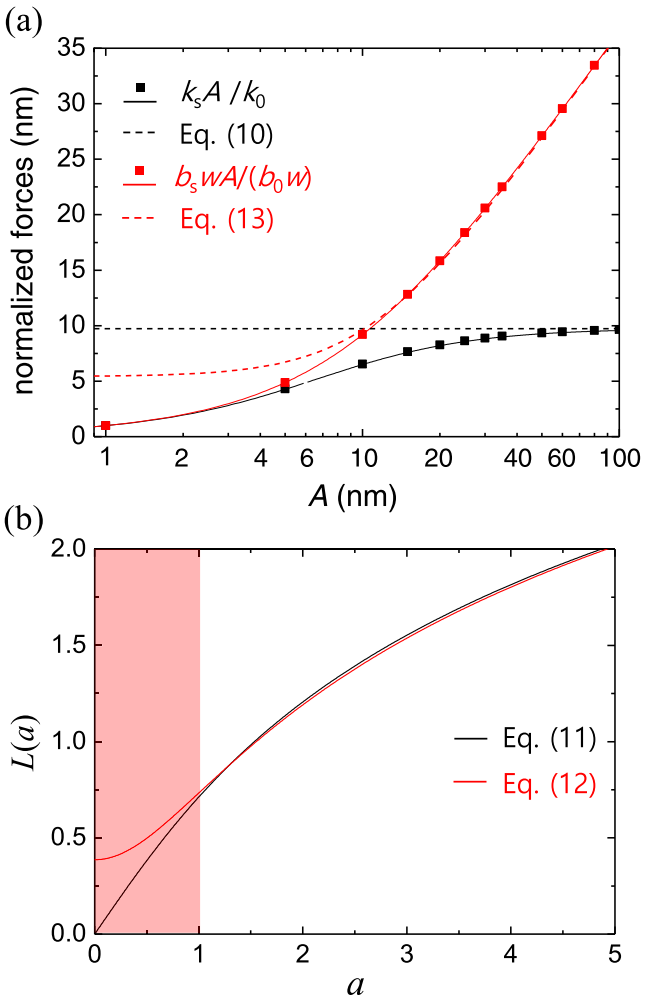

FIG. 4. Scaling behaviors of the magnitudes of elastic and damping forces, k_sA and b_swA, with the shearing amplitude A. (a) The magnitude of the elastic force k_sA converges to a finite value [Eq. (10)], whereas the damping component b_swA increases logarithmically with A. The black solid curve is from Eq. (6) and the red solid curve from Eq. (8). The black and red colored dots are the results obtained by using the data sets of colored dots in Fig. 3(b). (b) The function $L(a)$ [Eq. (11)] (black curve) is well approximated by Eq. (12) (red curve) for $a > 1$.

moving direction of the tip. Both the elastic and the damping forces [Eqs. (1) and (4)] increase linearly with the oscillation amplitude at small amplitude, but they change nonlinearly at large amplitude. This leads to the inclined elliptical shape of the shear-force curve [Eq. (5)] at small amplitude. The shape is distorted as the amplitude becomes larger [Fig. 3(a)].

The fluidic impedance, characterized by k_s and b_sw [Eqs. (6) and (8), and Supplemental Material [26]), is shown in Fig. 3(b). The elasticity k_s converges to k_0 and the damping coefficient b_sw converges to b_0w, as $A \to 0$. Since $k_s(A) \approx |F_k|/A$ and $b_swA \approx |F_b|/A$ approximately, the specific nonzero k_0 and b_0w imply that the forces F_k and F_b linearly increase with the amplitude A, and that the interaction coefficients k_s and b_sw are independent of the amplitude A for small A. Experimentally, these finite constant valued k_0 and b_0w are observed even at the amplitude of subnanometer scale [21]. This indeed indicates the molecular process at the contact line.

Surprisingly, the contact-line-induced damping impedance b_sw is about five orders of magnitude higher than the viscous damping caused by bulk-valued viscosity. Furthermore, the elasticity k_s is generated by the contact line, which is not induced by the viscosity of the fluid. The contact-line-induced damping b_0w [Eq. (9)] is about 1 N/m, but the viscous damping of a nanometric water bridge is estimated to be 10^{-5} N/m with bulk viscosity of water 1 mPa s, contact radius $R_\psi = 15$ nm, and height $h_\psi = 6$ nm. This shows that the effect of the contact line is significant for the overall interaction, although it is nanometer sized.

We find k_s decays faster than b_sw with increasing A [Fig. 3(b)]. This is because k_s is associated with the interfacial geometry [Eq. (1)] and b_sw with the sliding dynamics at the liquid-solid interface [Eq. (4)]. The liquid-vapor interfacial energy change, associated with the elastic force, does not infinitely increase but has a limited value under shear modulation. However, the damping force on the contact line persistently increases with shearing amplitude. These are consistent with previous experimental results [17].

The magnitude of the oscillatory elastic force k_sA converges to a finite value, as the amplitude increases. From Eq. (6), we get

$$\frac{k_sA}{k_0} = \frac{16}{\pi^2} \quad \text{as } A/h_\psi \to \infty, \tag{10}$$

where we have used the relations $(\pi^2/4)_3F_2[-\frac{1}{2}, \frac{1}{2}, \frac{1}{2}; 1, 1; -\overline{A}^2] \approx \overline{A}$ and $K[\frac{1}{2}(1 - \sqrt{1+\overline{A}^2})] \approx 0$ as $\overline{A} \equiv A/h_\psi \to \infty$. This convergence, observable in Fig. 4(a) (black dashed line), was also seen in experiments [17].

The magnitude of the damping force b_swA increases logarithmically with amplitude [red solid and dashed curves, Fig. 4(a)]. This behavior follows from the asymptotic relation

$$L(a) \equiv \frac{\sqrt{1+a^2}}{a}\left\{K\left[\frac{a^2}{1+a^2}\right] - E\left[\frac{a^2}{1+a^2}\right]\right\} \tag{11}$$

$$\approx \frac{1}{2}\ln(1+a^2) - \sigma - \psi^{(0)}(1/2) - 1 \quad \text{as } a \to \infty, \tag{12}$$

where σ is the Euler-Mascheroni constant and $\psi^{(0)}(1/2)$ is the Polygamma function of order 0 at a value 1/2. We use the approximation of $L(a)$ to derive the scaling behavior for b_swA [Eq. (8)] as follows:

$$\frac{b_swA}{b_0w} = \frac{8V_0e^{-U/k_BT}}{\pi w}\left\{\frac{1}{2}\ln(1+a^2) - \sigma - \psi^{(0)}(1/2) - 1\right\} \times \text{as } a \to \infty. \tag{13}$$

As shown in Fig. 4(b), Eq. (12) excellently represents $L(a)$ with a discrepancy of less than 3% for $a > 1$. Since $a = Aw/(2V_0e^{-U/k_BT})$, $a = 1$ corresponds to $A = 12$ nm. Further, $(1/2)\ln(1+a^2)$ approaches $\ln(a)$ for large a. Therefore, the damping force b_swA is expected to scale as $\ln a$ or $\ln A$ for $A > 12$ nm [Fig. 4(a)], as observed in the previous experimental study [17].

In conclusion, we have developed an analytical theory for shear capillary force, taking into account the liquid-solid contact line mechanics. Our theory captures quantitatively the characteristic features of the experimental results, thereby offering a means to study liquid-solid dynamic interaction at the nanoscale. In particular, one can investigate the activation energy U and hopping length λ for various nanometric liquids by measuring k_s and $b_s w$.

The shear capillary force would strongly affect the sliding friction between two macroscopic surfaces. Numerous capillary-condensed liquid bridges could be formed within the nanoscale gap between contact as well as noncontact asperities on the surfaces. They not only increase effectively the normal load in the system and thus the solid-solid contact friction, but also could induce directly friction via the shear capillary force. When the relative velocity of the two surfaces is vanishingly small, the shear capillary force will induce a restoring force as predicted by Eqs. (1) and (6), resulting in enhanced static friction. On the other hand, when the two surfaces move at a relative velocity, the shear capillary force will also induce a damping [Eqs. (4) and (8)], contributing to kinetic friction. Since there would exist numerous capillary bridges between two macroscopic surfaces in contact [33,34], the effect of shear capillary force could be significant.

This giant interaction on the contact line also provides a clue for resolving the longstanding issue of viscosity enhancement in nanoconfined water. Nanoconfined water measured with interfacial force microscopy [35], surface-force apparatus [30,31], and quartz tuning-fork sensors [20–24] has shown a giant fluidic impedance, which has been often interpreted as enhanced viscosity in the nanoconfined water. However, the experimental systems included liquid-solid contact lines, that must have contributed significantly to the overall interaction. Such contact-line interaction may explain the measured giant interaction with water in such systems without the need to assume viscosity enhancement.

The pinning-depinning dynamics of water molecules at the liquid-solid contact line is distinct from hydrodynamics in bulk phase, and the molecular dynamics of water would be associated with the molecular structure of interfacial water. Indeed, Uhlig and Garcia reported hydration layer structures on a crystalline surface in capillary-condensed bridges [36]. This suggests a layered structure of water that could be formed on shearing surface of the tip, in which the water molecules on the layered structure could exhibit very different behavior from usual viscous dynamics. Therefore, the giant shear viscoelastic interaction might be associated with the pinning-depinning mechanics of the interfacial hydration water. The shear capillary force, the lateral component of capillary interaction, should be taken into account when studying any systems involving capillarity [37].

This work was supported by National Research Foundation of Korea (NRF) grants funded by the Korea government (MSIT) (2020R1F1A1073628, 2022 Research Equipment Technician Training Program, 2018R1A6A9056986), and the Industrial Strategic Technology Development Program-Materials Parts Technology Development Program (20010963, Semiconductor Process High Efficiency CMP Slurry Refinement Filter Media and Development of High Functional Product Technology) funded by the Ministry of Trade, Industry & Energy (MOTIE), the Technology development Program (S3052830) funded by the Ministry of SMEs and Startups (MSS, Korea), and the Commercialization Promotion Agency for R&D Outcomes(COMPA) funded by the Ministry of Science and ICT (MSIT) (2022 Mirae 03-4, Drug Delivery Techniques Based on Scanning Probe Microscopy), Korea.

[1] L. Bocquet, E. Charlaix, S. Ciliberto, and J. Crassous, Nature (London) **396**, 735 (1998).
[2] F. Restagno, L. Bocquet, and T. Biben, Phys. Rev. Lett. **84**, 2433 (2000).
[3] J. Jang, G. C. Schatz, and M. A. Ratner, Phys. Rev. Lett. **92**, 085504 (2004).
[4] B. N. J. Persson, *Sliding Friction: Physical Principles and Applications* (Springer-Verlag, Berlin, 2000)
[5] E. Riedo, F. Lévy, and H. Brune, Phys. Rev. Lett. **88**, 185505 (2002).
[6] R. Szoszkiewicz and E. Riedo, Phys. Rev. Lett. **95**, 135502 (2005).
[7] O. Noel, P.-E. Mazeran, and H. Nasrallah, Phys. Rev. Lett. **108**, 015503 (2012).
[8] H. Gouin, Colloids Surf. A **383**, 17 (2011).
[9] L. Sirghi, Appl. Phys. Lett. **82**, 3755 (2003).
[10] P. Barthelemy, M. Ghulinyan, Z. Gaburro, C. Toninelli, L. Pavesi, and D. S. Wiersma, Nat. Photonics **1**, 172 (2007).
[11] Z. Gaburro, M. Ghulinyan, L. Pavesi, P. Barthelemy, C. Toninelli, and D. Wiersma, Phys. Rev. B **77**, 115354 (2008).
[12] A. Vasudev and J. Zhe, Appl. Phys. Lett. **93**, 103503 (2008).
[13] P. Lambert, F. Seigneur, S. Koelemeijer, and J. Jacot, J. Micromech. Microeng. **16**, 1267 (2006).
[14] J. A. Fan, C. Wu, K. Bao, J. Bao, R. Bardhan, N. J. Halas, V. N. Manoharan, P. Nordlander, G. Shvets, and F. Capasso, Science **328**, 1135 (2010).
[15] V. N. Manoharan, M. T. Elsesser, and D. J. Pine, Science **301**, 483 (2003).
[16] H. J. Butt and M. Kappl, Adv. Colloid Interface Sci. **146**, 48 (2009).
[17] M. Lee, B. Kim, J. Kim, and W. Jhe, Nat. Commun. **6**, 7359 (2015).
[18] J. F. Louf, Y. Zheng, A. Kumar, T. Bohr, C. Gundlach, J. Harholt, H. F. Poulsen, and K. H. Jensen, Phys. Rev. E **98**, 042403 (2018).
[19] Y. Tang, H. Tang, J. Li, S. Zhang, B. Zhuang, and Y. Sun, Appl. Therm. Eng. **115**, 1020 (2017).
[20] H. Choe, M.-H. Hong, Y. Seo, K. Lee, G. Kim, Y. Cho, J. Ihm, and W. Jhe, Phys. Rev. Lett. **95**, 187801 (2005).
[21] M. Lee, B. Sung, N. Hashemi, and W. Jhe, Faraday Discuss. **141**, 415 (2009).

[22] S. An, J. Kim, K. Lee, B. Kim, M. Lee, and W. Jhe, Appl. Phys. Lett. **101**, 053114 (2012).
[23] B. Kim, S. Kwon, G. Moon, and W. Jhe, Phys. Rev. E **91**, 032307 (2015).
[24] H. Choe, D. Kim, M. Lee, and M. Choi, New Physics: Sae Mulli **71**, 439 (2021).
[25] W. Thomson, Nature (London) **34**, 270 (1886).
[26] See Supplemental Material at http://link.aps.org/supplemental/10.1103/PhysRevE.105.065108 for derivation of the equations.
[27] J. N. Israelachvili, *Intermolecular and Surface Forces* (Academic, London, 2003).
[28] T. D. Blake and J. M. Haynes, J. Colloid Interface Sci. **30**, 421 (1969).
[29] S. Gómez-Moñivas, J. J. Sáenz, M. Calleja, and R. García, Phys. Rev. Lett. **91**, 056101 (2003).
[30] J. Crassous, E. Charlaix, and J.-L. Loubet, Phys. Rev. Lett. **78**, 2425 (1997).
[31] Y. Zhu and S. Granick, Phys. Rev. Lett. **87**, 096104 (2001).
[32] M. Lee and W. Jhe, Phys. Rev. Lett. **97**, 036104 (2006).
[33] R. Sahli, G. Pallares, C. Ducottet, I. E. Ben Ali, S. Al Akhrass, M. Guibert, and J. Scheibert, Proc. Natl. Acad. Sci. USA **115**, 471 (2018).
[34] S. M. Rubinstein, G. Cohen, and J. Fineberg, Nature (London) **430**, 1005 (2004).
[35] R. C. Major, J. E. Houston, M. J. McGrath, J. I. Siepmann, and X.-Y. Zhu, Phys. Rev. Lett. **96**, 177803 (2006).
[36] M. R. Uhlig and R. Garcia, Nano Lett. **21**, 5593 (2021).
[37] M. Scheel, R. Seemann, M. Brinkmann, M. Di Michiel, A. Sheppard, B. Breidenbach, and S. Herminghaus, Nat. Mater. **7**, 189 (2008).